Surface Roughness Characterizations of Sea Ice and Ice Sheets: Case Studies With MISR Data

Anne W. Nolin, Florence M. Fetterer, *Member, IEEE*, and Theodore A. Scambos

***Abstract*—This work is an examination of potential uses of multiangular remote sensing imagery for mapping and characterizing sea ice and ice sheet surfaces based on surface roughness properties. We use data from the Multi-angle Imaging SpectroRadiometer (MISR) to demonstrate that ice sheet and sea ice surfaces have characteristic angular signatures and that these angular signatures may be used in much the same way as spectral signatures are used in multispectral classification. Three case studies are examined: sea ice in the Beaufort Sea off the north coast of Alaska, the Jakobshavn Glacier on the western edge of the Greenland ice sheet, and a region in Antarctica south of McMurdo station containing glaciers and blue-ice areas. The MISR sea ice image appears to delineate different first-year ice types and, to some extent, the transition from first-year to multiyear ice. The MISR image shows good agreement with sea ice types that are evident in concurrent synthetic aperture radar (SAR) imagery and ice analysis charts from the National Ice Center. Over the Jakobshavn Glacier, surface roughness data from airborne laser altimeter transects correlate well with MISR-derived estimates of surface roughness. In Antarctica, ablation-related blue-ice areas, which are difficult to distinguish from bare ice exposed by crevasses, are easily detected using multiangular data. These unusual ablation surfaces are smooth and, unlike nearby crevassed ice, are strongly forward scattering. These case studies demonstrate that MISR data can make an innovative and important contribution to remote sensing of ice sheet and sea ice surface properties.**

***Index Terms*—Antarctica, Beaufort Sea, blue-ice areas, Greenland, ice sheets, Multi-angle Imaging SpectroRadiometer (MISR), sea ice, surface roughness.**

I. Introduction

OPTICAL remote sensing using simultaneously acquired multiangular data is a relatively new concept. Most classification algorithms rely on variations in spectral reflectance. However, recent research indicates that anisotropic scattering from various earth surface types (e.g., soil, vegetation, cloud, and snow) creates characteristic angular signatures in addition to the better known spectral signatures [1]–[3]. Subscale surface roughness is the surface texture having length scales finer than can be resolved by a particular satellite-based sensor. Herzfeld *et al.* [4] define it as the derivative of surface microtopography. Surface roughness affects both the spectral reflectance, through subpixel shadowing, and the angular distribution of reflected radiance. Rougher surfaces are backward scattering, even when the material itself may be predominantly forward scattering. For example, ice is forward scattering at the particle scale, but at larger scales, surface microtopography such as sastrugi (wind-eroded snow) and glacier crevasses are backward scattering [5], [6]. If the surface texture is indicative of the state of the material, it follows that multiangular measurements may be used for morphological classification of the snow or ice surface. This relationship between backscattering and surface morphology has been exploited by synthetic aperture radar (SAR) and SAR interferometry for mapping sea ice types [7], [8] and ice sheet topography [9]–[12]. However, to date, multiangular approaches using optical remote sensing data have not been applied to mapping sea ice and ice sheet surface roughness.

The Multi-angle Imaging SpectroRadiometer (MISR) is an innovative instrument that uses simultaneous multiangular measurements to obtain angular reflectance information for retrieval of geophysical parameters [13]. In this work, we use MISR imagery of three case study areas to identify potential ways in which multiangular data can help characterize surface roughness on ice sheets and sea ice.

The primary objective of this research is to demonstrate the utility of using multiangular measurements over sea ice and ice sheets to detect changes in subpixel scale roughness that are relevant to their classification. Specifically, we aim to examine 1) whether angular signatures may be used to distinguish between sea ice types and 2) how well angular patterns correspond to ice sheet surface roughness.

II. MISR Data Description

The MISR instrument was launched in December 1999 on board NASA's Terra satellite. It is a pushbroom sensor, with nine cameras aligned in the along-track direction and four spectral bands per camera. The sensor has high radiometric resolution (14-bit quantization) and a broad radiometric range, so that it does not saturate over bright targets such as snow and ice. Over a 7-min interval, the subspacecraft location is sequentially viewed by each of the nine MISR cameras. Thus, for a particular overpass each pixel is viewed at essentially the same solar geometry but nine different viewing angles.

The MISR instrument acquires a suite of 36 reflectance measurements (nine cameras $\times$ four channels) providing both spectral and angular information. The spatial resolution of the instrument depends on the camera and the channel. All cameras have the red channel at 275-m spatial resolution. The nadir camera has all four channels at 275-m spatial resolution. The blue, green, and near-infrared channels in the other cameras

Manuscript received September 10, 2001; revised May 2, 2002. This work was supported in part by NASA under Grant NAG5-6462.

The authors are with the National Snow and Ice Data Center, Cooperative Institute for Research in Environmental Sciences, University of Colorado, Boulder, CO 80309 USA (e-mail: nolin@spectra.colorado.edu; fetterer@kryos.colorado.edu; teds@icehouse.colorado.edu).

Publisher Item Identifier 10.1109/TGRS.2002.801581.

TABLE I
DESCRIPTION OF THE MISR INSTRUMENT

Camera Angles	±70.5°, ±60.0°, ±45.6°, ±26.1°, 0°
Spectral Bands	448 nm (Blue), 558 nm (Green), 672 nm (Red), 866 nm (near IR)
Pixel Size	275 × 275 m (all bands in nadir camera and red bands in all other cameras) 1.1× 1.1 km (blue, green, and near IR bands in fore and aft cameras)
Swath width	380 km
Quantization	14 bits, square-root encoded to 12 bits

TABLE II
DESCRIPTION OF MISR IMAGERY USED IN THE THREE CASE STUDIES

Location	Date	Orbit Number	Center Lat/Lon
Beaufort Sea	19 March 2001	6663	72.0°N, 145.0°W
Jakobshavn Glacier	4 May 2001	7329	69.5°N, 48.5°W
	5 June 2001	7795	
	7 July 2001	8261	
East Antarctica	27 January 2001	5916	79.6°S, 159.2°W

have a resolution of 1.1 km (see Table I). MISR geolocation accuracy is excellent with root-mean-square (rms) errors ranging from 143 m (nadir camera) to 350 m (70.5° aft camera) in the along-track direction and from 115 m (nadir camera) to 160 m (70.5° aft camera) in the cross-track direction.

III. CASE STUDY AREAS: SIGNIFICANCE AND DESCRIPTION

We have chosen three locations for this study: sea ice in the Beaufort Sea, the Jakobshavn Glacier in western Greenland, and an area in eastern Antarctica with glaciers and exposed blue ice. The three study areas were selected for several reasons. Each of the areas has been the subject of previous studies; each has some particular cryospheric significance; and each exhibits spatial and/or temporal changes in surface roughness that make it a useful candidate for multiangular classification. Table II summarizes the MISR images used for each case study area.

A. Sea Ice

Sea ice acts as the dominant control on ocean–atmosphere fluxes in the polar oceans and is a climatically sensitive part of the earth system. Recent research has suggested that sea ice concentrations have decreased in the Arctic and possibly the Antarctic [14]–[18]. Regionally, the western Arctic appears to be experiencing significant decreases in the average thickness of ice [19], [20], implying a change in sea ice mass balance. Information on sea ice extent, concentration, and thickness is also needed for high-latitude navigation. Of particular importance is the extent of multiyear ice (sea ice that has survived one or more summers), since this indicates ice that is substantially thicker than first-year ice (ice which forms during the winter and melts in the summer). Decreased salinity also occurs in multiyear ice, as brine is removed from the ice over time. Multiyear ice tends to have an undulating surface because of the formation of melt ponds and their subsequent draining and/or refreezing. First-year ice is relatively smooth except where ridging and cracks have occurred.

Satellite remote sensing has long been used to map sea ice. These tools include passive sensors that measure microwave emission or reflected sunlight as well as active sensors that measure radar backscatter. Visible and near-infrared imagery offer good spatial resolution, typically at scales of 1 km or finer. However, problems with cloud cover make the all-weather contributions of microwave sensors very attractive. Though relatively insensitive to clouds, passive microwave data are limited in their ability to determine sea ice types, and their resolution is fairly coarse (about 25 km). In summer, ice concentration is underestimated due to the presence of surface melt water and other effects [21]. Another difficulty is that sea ice within approximately 50 km of the coast is not accurately mapped because of the effects of mixed land–ocean pixels. Satellite SAR imagery, which measures radar backscatter, is an important tool for operational sea ice monitoring [22]. SAR has the advantages of high resolution (25-m to 100-m resolution is generally used for sea ice monitoring) combined with a relatively wide swath (500 km for RADARSAT ScanSAR mode) and the ability to image the surface through darkness, clouds, and dry snow. The RADARSAT Geophysical Processing System [23] uses SAR imagery to produce gridded fields of ice motion and ice thickness (based on a model of ice growth, divergence from motion fields, and freezing degree day information). The U.S. National Ice Center (NIC) uses a variety of satellite data, aircraft reconnaissance data, and model estimates to produce charts of weekly sea ice concentrations, stages of ice development, and forms of sea ice [24]. The high level of detail in NIC regional products results primarily from manual analysis of SAR data.

Backscatter in SAR imagery (i.e., the strength of the radar return) depends on surface roughness as well as the dielectric constant of the reflecting material. Much of the early work on using SAR for sea ice-type mapping attempted to model backscatter in terms of these parameters and to equate backscatter with ice types ([25] provides an overview; also see [26]). Multiyear ice has a relatively low dielectric constant because of its low salinity, and it appears bright in SAR imagery as a result of reflections off bubbles within the ice as well as from its rough surface. Thinner ice types appear darker because they are more saline and have a higher dielectric constant that prevents radar energy from penetrating the ice surface. Thinner (and younger) ice types have not been exposed to weathering and other forces that roughen the surface. Their smooth surface tends to specularly reflect the radar signal, so young ice types generally appear dark in SAR imagery.

Because both SAR and MISR imagery register surface roughness, albeit at different scales and in a different manner, we expect some similarities. Backward and forward scattering are both relative to the source of illumination. In the case of MISR, forward scattering is that which is directed away from the sun, and backward scattering is directed back into the direction of the sun. Rougher old ice that is bright in SAR imagery (because of surface roughness as well as inclusions such as air bubbles and brine pockets) would also be expected to show greater backward scattering in MISR imagery (because of surface roughness alone). Smoother, younger ice types that usually appear dark in SAR imagery would be expected to be predominantly forward scattering in MISR imagery. Younger ice types have backscatter

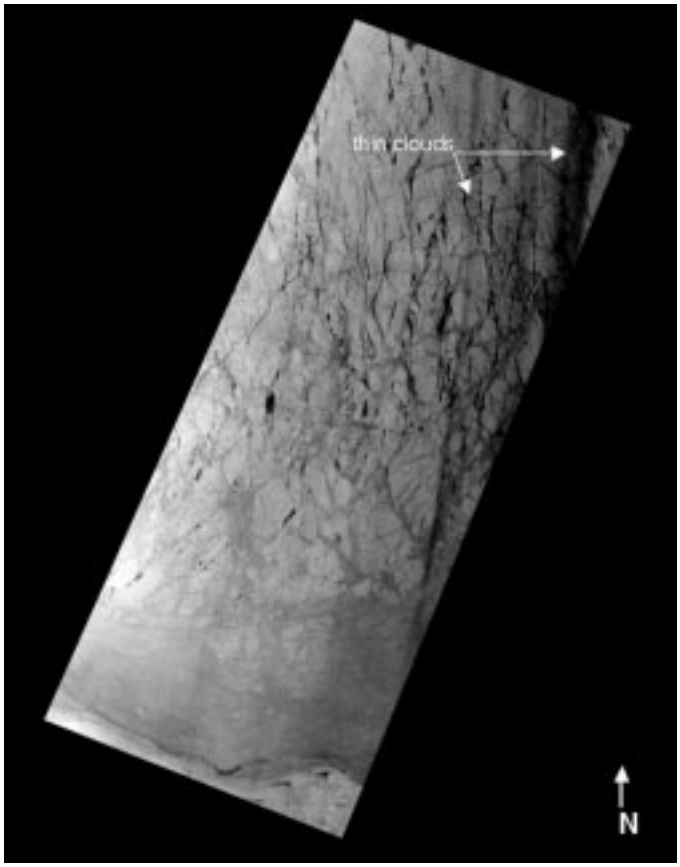

Fig. 1. MISR nadir red channel image of sea ice off the north coast of Alaska. The image was acquired on March 19, 2001. This image strip covers an area of 200 km × 800 km.

signatures that overlap in SAR data [27], and the thinnest ice types have signatures that are below the noise floor of spaceborne SAR [28]. With SAR, sea ice surface roughness is detectable at the centimeter scale, comparable to the wavelength of the sensor. For MISR, detection of surface roughness depends on the wavelength of the roughness as well as the solar illumination and viewing geometries. The quantitative relationship between roughness and detectability has not yet been established for MISR. Additional work will be needed to explore this. Here, we show only that MISR angular reflectance signatures demonstrate the expected differences in ice surface roughness based on ice type.

Our sea ice case example is in the Beaufort Sea, off the north coast of Alaska. This location was selected because of the presence of both multiyear and first-year sea ice types. We use MISR and RADARSAT images acquired on March 19, 2001, at which time both multiyear and first-year ice types are present but prior to the onset of surface melt. Fig. 1 is a nadir camera, red channel image from MISR showing the coast of Alaska at the bottom of the image with first-year and multiyear ice to the north. Some thin clouds are present on the east side of the image. We interpret the MISR image using a concurrent RADARSAT image and NIC ice analysis charts as "truth." Confidence in the NIC product is based on NIC's methods of analysis (manual image interpretation by an analyst who specializes in the region) and data sources (satellite imagery, as well as models and ship and shore observations).

B. Greenland Ice Sheet

The vast ice sheets of Greenland and Antarctica contain approximately 77% of our planet's fresh water [29]. Trends in accumulation, ablation, and ice dynamics affect the overall mass balance of the ice sheet and contribute to changes in global sea level. Although their potential impact on sea level rise is undisputed, there is uncertainty in the mass balance of these large and remote ice sheets. Numerous studies over the past two decades paint an incomplete picture of complex interactions between climate, ice sheet accumulation/ablation, and ice dynamics [30]–[33]. Passive microwave measurements have recorded overall increases in the melt region over the past 25 years [34]. Laser altimeter measurements show overall ice sheet mass balance at elevations above about 2000 m, rapid thinning along the eastern margin of the ice sheet, and thickening of some outlet glaciers along the western coast [35], [36]. The dramatic thinning evident in many of the outlet glaciers cannot be completely explained by changes in ice ablation and accumulation, implying that a change in ice dynamics is involved. Surface roughness comes into play in the sense that surface morphology is a record of combined effects of snow accumulation, ablation, and ice movement. An increase in melt area will lead to an incursion of melt ponds into previously smooth regions of the ice sheet. Changes in wind erosion and sublimation will affect sastrugi and snow dune formations in the dry-snow zone. Structures such as glacier crevasses and ice surges provide a record of ice dynamics.

Although optical remote sensing is limited to the sunlit season, changes in surface roughness zones are best observed in summer when ablation processes are dominant. Cloudiness can inhibit the use of optical data, but at high latitudes, the temporal coverage is frequent. For MISR, temporal coverage poleward of 60° latitude is at least one image every five days, so cloud-free images of a region can be regularly obtained.

Our study area is in western Greenland, over the Jakobshavn Glacier and its upland drainage basin. This particular glacier is important because it drains a significant portion of the western Greenland ice sheet, has the fastest flow on the ice sheet, and has high rates of iceberg calving. Previous work [4], [37] has mapped distinct morphogenetic provinces along the glacier, based on surface roughness patterns measured using SAR data, video imagery, and ground-based measurements. These roughness zones correspond to different surface processes that affect the glacier (development of sastrugi, formation of melt ponds, crevassed areas, etc.). Fig. 2 is a nadir red channel MISR image of the Jakobshavn Glacier on May 4, 2001. The glacier, in the left portion of the image, is characterized by crevassed ice as it nears its outlet. Spectrally, this crevassed portion of the glacier is darker than the upland drainage region because of the self-shadowing effects of the deep crevasses [5]. The upper portion of the Jakobshavn Glacier drainage basin, on the right side of the image, is characterized by high snow accumulation [30], [31], [33]. The intermediate portions of the drainage basin have melt ponds and, later in the summer, bare ice. Our goal with this case study is to see if MISR data may be used to map surface roughness that could be used in future work to classify and monitor morphogenetic provinces associated with these important outlet glaciers.

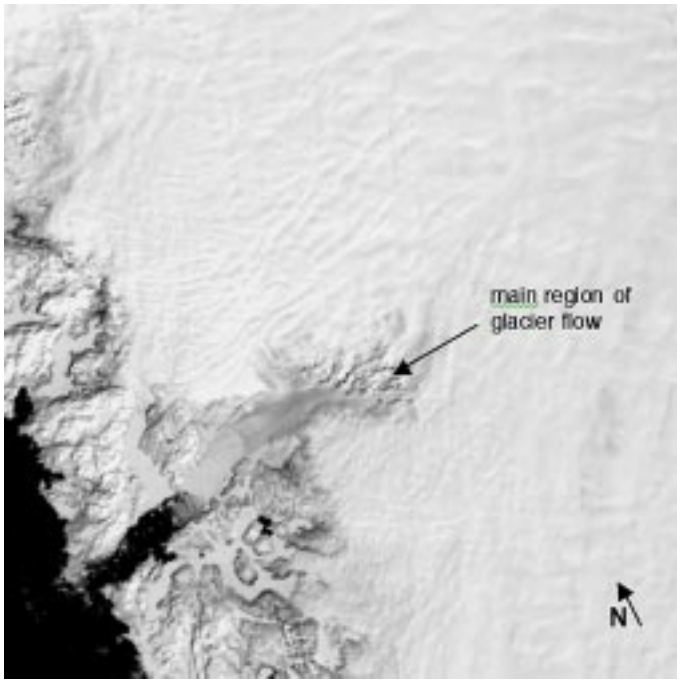

Fig. 2. MISR nadir red channel image of the Jakobshavn Glacier in western Greenland. The image was acquired on May 4, 2001 and covers an area of 137.5 km × 137.5 km. The Jakobshavn Glacier flows into a narrow channel ("isbræ") where it releases substantial numbers of icebergs from its terminus. The dark area in the lower leftcorner is ice-free ocean. The rugged coastline is covered with snow at this time of year.

C. Antarctic Blue-Ice Areas

In Antarctica, extremely dry and windy conditions result in large areas of net ablation on the ice sheet, known as "blue-ice areas" [38]. Net ablation, i.e., negative surface mass balance, causes the surface layers of seasonal snowfall and old firn to be removed primarily through sublimation, exposing dense older ice beneath [39]–[41]. Because of this, concentrations of meteorites collect on the surface of blue-ice areas [42], [43]. They also tend to be flat, hard surfaces and have been used as aircraft landing strips [44]. Furthermore, because of the expected sensitivity of these regions to changes in climate, particularly at their edges, recent studies have attempted to map blue-ice extent as a baseline for future climate change monitoring [45]–[47]. Preliminary attempts at mapping blue-ice areas have used multispectral optical imagery, based on the very distinctive differences in the visible and near-infrared spectral reflectance of blue ice and snow [45], [47]. However, multispectral approaches cannot distinguish between ablation-exposed blue ice and areas where deep crevassing exposes blue ice (and so, in current maps, crevassed areas are manually masked based on glaciological guessing). Blue ice that is exposed in glacier crevasses is the result of the combined processes of ablation and ice flow. Therefore, we want to distinguish between blue ice in crevasses and smooth blue ice in order to better isolate the climate signal. We examine the possibility of using the very large differences in surface roughness between the two surface types, in concert with their distinct spectral signature relative to snow, as a means of more accurately and more automatically mapping blue-ice extent.

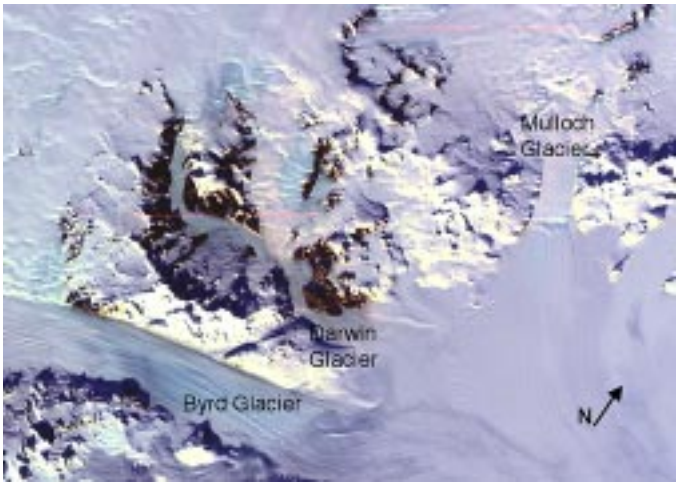

Fig. 3. MISR true-color image of blue-ice areas and glaciers south of McMurdo station, Antarctica. The image was acquired on January 27, 2001 and covers an area of 250 km × 200 km. The three main glaciers shown in the image flow down into the Ross Ice Shelf, which comprises the lower right portion of the image.

Fig. 4. Blue-ice surface in the foreground exhibits strong forward scattering. This photo is of the area called "Meteorite Hills," after the large number of meteorites found on its surface. (Photo courtesy Larry Nittler, Carnegie Institute, Washington, D.C.)

Extensive regions of ablation-derived blue-ice exposure and adjacent major outlet glaciers just south of McMurdo Station, Antarctica are our third study area. Fig. 3 shows a true-color composite MISR image acquired on January 27, 2001. The snow-covered Ross Ice Shelf is in the lower right portion of the image. The Byrd, Darwin, and Mulloch glaciers flow eastward from the East Antarctic plateau into the Ross Ice Shelf. On the flanks of the upper reaches of these glaciers are large areas of ablation-derived blue ice. These particular areas, the Darwin, Bates, and Butcher Ridge ice fields, are the site of meteorite collection efforts [43] due to meteorite concentration on the surface by thousands of years of ice flow and ablation. Rock outcrops surround the glaciers and ablation areas. Fig. 4 is a photograph of a blue-ice area known as "Meteorite Hills" and is also shown in the MISR image. This photograph was taken

looking toward the sun and shows the strong forward scattering off the relatively smooth ice surface.

IV. Methodology

The three study areas are treated somewhat differently, since the objectives and the ancillary data used for assessment of the MISR results are different in each case. For all locations we use mostly cloud-free MISR data.

In this work, we convert the top-of-atmosphere (TOA) scaled radiances to TOA reflectance values. This yields a quantity termed the bidirectional reflectance factor (BRF), which is the ratio of the reflected light in the direction of the sensor to that of the incident solar beam. The two directions implicit in the term "bidirectional" are the illumination and viewing directions, where the illumination is the direct beam solar irradiance. When there is some proportion of diffuse illumination, such as at the surface, the term hemispherical-directional reflectance factor (HDRF) is used, since the illumination is hemispherical and the observation is directional. Thus, for TOA measurements, it is the BRF that describes the reflectance while, for surface measurements, HDRF is the correct term. In this work, TOA BRFs are used rather than surface HDRFs because atmospheric effects do not significantly modify angular signatures of bright snow and ice surfaces. Furthermore, atmospheric profile data on water vapor, ozone, and aerosols are sparse or nonexistent over the case study regions, preventing accurate atmospheric correction of MISR imagery.

A. Beaufort Sea Ice

To assess the effectiveness of MISR data for distinguishing between sea ice types, we use a RADARSAT SAR image acquired on the same day as the MISR overpass. The NIC ice analysis chart for the week of March 19–23, 2001 is also used to identify boundaries between first-year ice types and multiyear ice. A multiangular classification of the image is performed using the red channel reflectances at MISR's nine camera angles.

We use an iterative self-organizing data analysis (ISODATA) unsupervised classifier [48] to determine the number of classes in the MISR image and their spatial distribution. This commonly used clustering technique uses an initial cluster vector and then iteratively assigns pixels to the closest cluster based on distance from the cluster mean. The ISODATA algorithm minimizes the within-cluster variability but does so without any *a priori* assumption of the final number of clusters. Both the classified image and the RADARSAT image are georeferenced to a UTM coordinate system. Regions in the classified image are then compared with the RADARSAT backscatter image and the NIC ice analysis chart.

B. Jakobshavn Glacier

To map surface roughness in our second case study area, we use MISR forward and backward pointing cameras and compare these measurements with colocated laser altimeter measurements of surface roughness. Since the MISR data are not a direct measure of ice sheet surface roughness, we have developed a proxy for this parameter, created by computing a normalized difference angular index (NDAI)

$$\mathrm{NDAI} = (\mathrm{back} - \mathrm{fore})/(\mathrm{back} + \mathrm{fore}) \tag{1}$$

where, back is the backward-scattered radiance at MISR's -70.5° viewing angle and fore is the forward-scattered radiance at the $+70.5^\circ$ viewing angle. The normalization process removes pixel-to-pixel illumination differences. Bright pixels in an NDAI image indicate strong backward scattering associated with rough surfaces, while smoother areas will be predominantly forward scattering. For comparison with these MISR-derived estimates of ice sheet surface roughness, we use data acquired on May 15, 1997 from the Airborne Topographic Mapper (ATM). The ATM is a scanning airborne laser altimeter that collects highly accurate elevation data. With its high scan rate, the ATM collects a dense set of elevation measurements along a 140-m-wide swath. Root-mean-square accuracy of elevations is 10 cm or better. The elevation data are resampled to 70-m planes using a best fit technique. The rms error of the fit of the data to the plane is the surface roughness. Although the ATM data are not concurrent with the MISR imagery, they are from the same time of the sunlit season (mid-May). Since these data were acquired prior to the onset of melt (which varies from year to year), they will reflect the early-season surface roughness, which has much lower year-to-year variability.

Both the MISR and the ATM data are georeferenced, allowing the ATM transects to be overlaid as vector data on the MISR NDAI image. NDAI values from the corresponding MISR pixels are then extracted. Because the data ranges of the two are different, we rescale the data by subtracting the mean and dividing by the standard deviation. Data from the three MISR images, spaced about one month apart, are used to identify changes in surface roughness over the course of the 2001 summer season from May to July 2001.

C. Blue-Ice Areas in East Antarctica

Landsat Thematic Mapper (TM) data are used to map blue-ice areas in the vicinity of the Darwin and Byrd Glaciers in East Antarctica. Previous ground-based surveys [43] have indicated the compositional similarity between the smooth blue-ice areas adjacent to the rock outcrops and the blue ice that is exposed in glacier crevasses such as on the Byrd Glacier. Such material similarities and morphological dissimilarities have also been mentioned for other blue-ice regions in Antarctica [47].

MISR data processing employed the NDAI to identify smooth blue ice and distinguish it from blue ice in glacier crevasses. To emphasize the blue spectral peak [49] of the blue ice, we use a blue-red normalized difference (BRND), similar to the NDAI but using the blue and red channels of MISR's nadir viewing camera. To emphasize the difference in grain size between blue ice and snow, we use an IR-blue normalized difference (IBND). Snow with a large grain size has lower infrared reflectance and, therefore, a smaller difference between infrared and blue channels [50], [51]. When compared with snow, blue ice has a very large effective grain size.

In addition, we examine the angular signatures of the blue ice and crevassed regions. Because we are interested in the relative

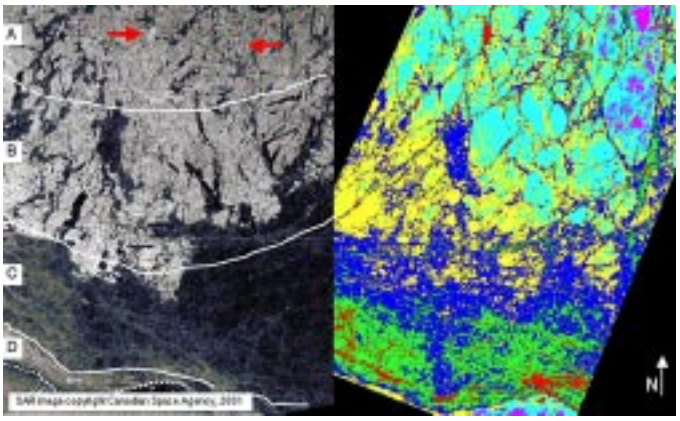

Fig. 5. (Left) RADARSAT image at 100-m spatial resolution acquired on March 19, 2001. The image covers an area of 185 km × 300 km. Solid white lines from the NIC ice charts and marks areas of predominantly multiyear ice (A) and various forms of first-year ice (B)–(D). The dotted white line at the bottom marks the coastline. (Right) Classified MISR image from the same day. Blue, green, red, and yellow pixels correspond to various types of first-year ice. Cyan pixels match the area that is composed of predominantly multiyear ice flows. Magenta pixels are thin clouds. The red arrows indicate frost flowers with distinctive scattering properties that can be seen in both images.

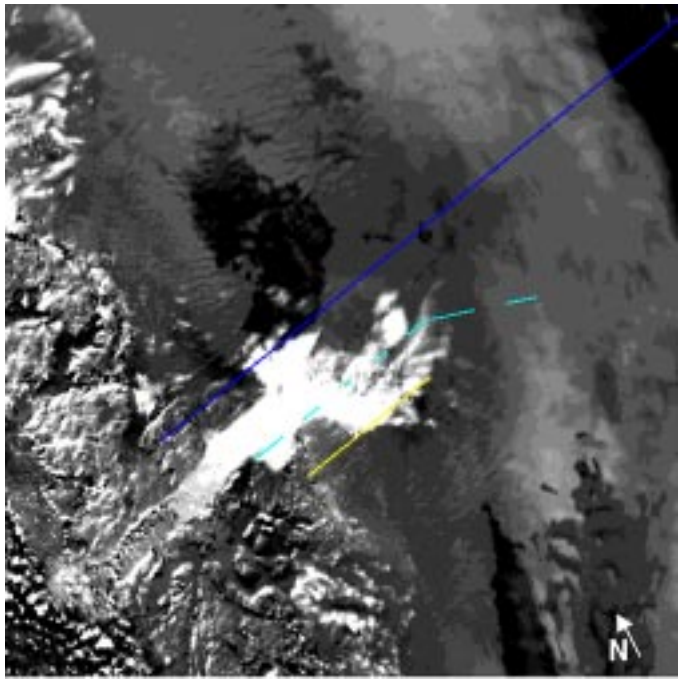

Fig. 6. MISR normalized difference angular index image for May 4, 2001. North, center, and south transects are shown in blue, cyan, and yellow, respectively. Bright areas indicate strong backward scattering, while darker areas show predominantly forward scattering.

magnitude of BRFs as a function of viewing angle (or, for spectral evaluation, channel) we normalize using the following:

$$\mathrm{BRF}_{\mathrm{norm}} = \mathrm{BRF} - \frac{\sum_{i=0}^{n} \mathrm{BRF}}{n} \tag{2}$$

where $\mathrm{BRF}_{\mathrm{norm}}$ is the normalized BRF value and n is the number of values included in the measurement of the signature ($n = 9$ for angular measurements; $n = 4$ for spectral measurements).

V. Results

A. Sea Ice in the Beaufort Sea

Fig. 5 shows the results of the ISODATA classification of the MISR image, alongside an SAR image of the same area. ISODATA is an efficient way of determining whether the nine input channels contain angular information related to sea ice type (much of the information is redundant, and further work would be needed to determine the optimal combination of channels for discriminating ice types). The ISODATA routine found five classes for sea ice (magenta is related to land and cloud). Cyan maps most multiyear floes (judging multiyear by the bright signature in the SAR image and the delineation of multiyear ice on the NIC chart). Blue and green map first-year and younger types. Red maps thin ice, which is dark in the nadir MISR image (Fig. 1) and is often very bright, due to the formation of large, multicrystal and angular faceted "frost flowers" on the surface [25], in the SAR image. (The red arrows on the SAR image mark two of these features.) Yellow maps a mixture of multiyear and younger ice types that roughly corresponds to the boundary in the SAR image between the bright regions and the dark region. This also roughly corresponds to the boundary shown in the NIC ice chart. The angular signature classified as yellow reflects surface roughness differences with the surrounding ice that are apparently not a definitive reflection of the underlying ice type or morphology. Based on examination of the angular signatures (not shown), the red-classified regions are forward scattering, while blue-classified areas are more backward scattering. The other classes have statistically distinct angular signatures and fall into the middle of the forward/backward scattering continuum.

Because SAR penetrates dry snow and into old ice, while the optical MISR sensor measures reflectance at the surface, which may be snow-covered, we can only expect a gross correspondence between angular signatures from MISR and SAR backscatter. We do find this: younger types tend to be forward scattering in MISR and dark in SAR (with the exception of new ice covered by frost flowers), while multiyear ice tends for be backward scattering and bright in SAR. Linear features in the upper portion of the MISR image represent thinner first-year ice between large floes of multiyear ice. These features do not appear in the SAR image, since SAR is not sensitive to these small differences. At present, MISR imagery offers few advantages over SAR for operational ice mapping, but can complement SAR by, for example, resolving areas of very thin ice that may be confused with multiyear ice in SAR. MISR may also be useful in summer, when surface melt makes it difficult to distinguish between sea ice and open water in SAR imagery, and passive microwave ice concentration data are also unreliable.

B. Jakobshavn Glacier in Western Greenland

Comparisons between MISR NDAI values and colocated ATM surface roughness values show generally good agreement between the two. Figs. 6–8 show the normalized difference images for the three dates (May 4, June 5, and July 7, 2001) with the superimposed locations of the laser altimeter transects. In the May image, the lower portion of the glacier exhibits

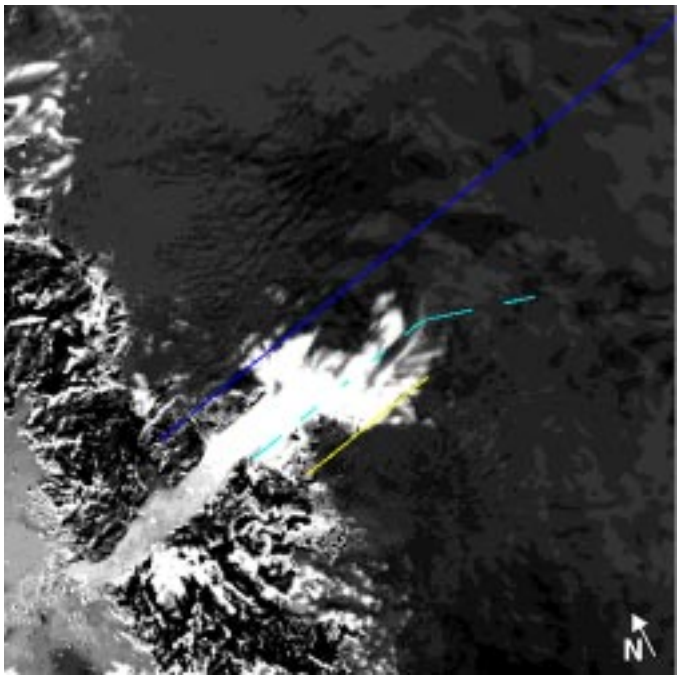

Fig. 7. MISR normalized difference angular index image for June 5, 2001. Melt has started in the lower regions of the glacier, and coastal areas that were previously snow-covered are becoming exposed.

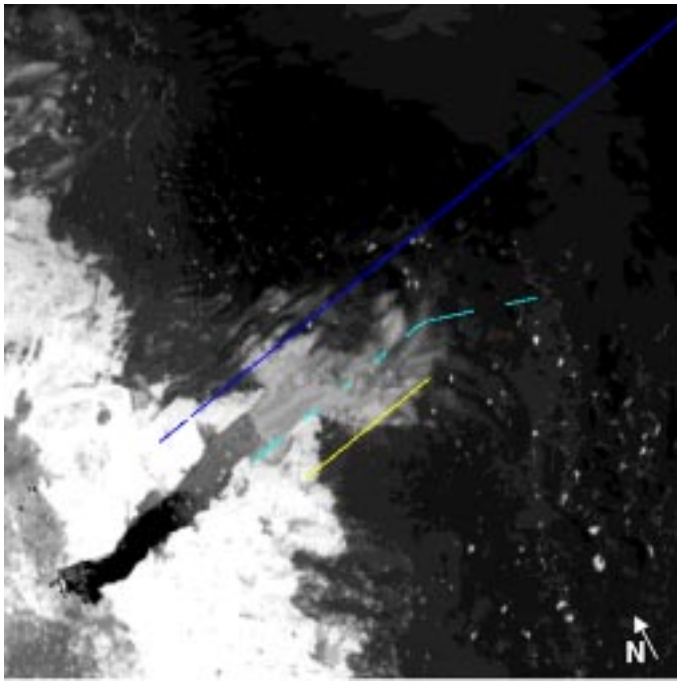

Fig. 8. MISR normalized difference angular index image for July 7, 2001. Melt ponds have formed over an extensive area (white, backscattering stippled area). The coastal area is now devoid of snow and appears much rougher than in earlier images. The calving front of the glacier is clearly indicated with floating ice and icebergs present downstream of the glacier terminus. The upland areas of the drainage basin are still predominantly forward scattering.

strong backward scattering from the heavily crevassed ice. Coastal pixels are snow-covered and so are only moderately backward scattering. The upper reaches of the glacier drainage basin are mostly forward scattering. In later images, the coastal areas lose their snow cover and appear rough. By early July,

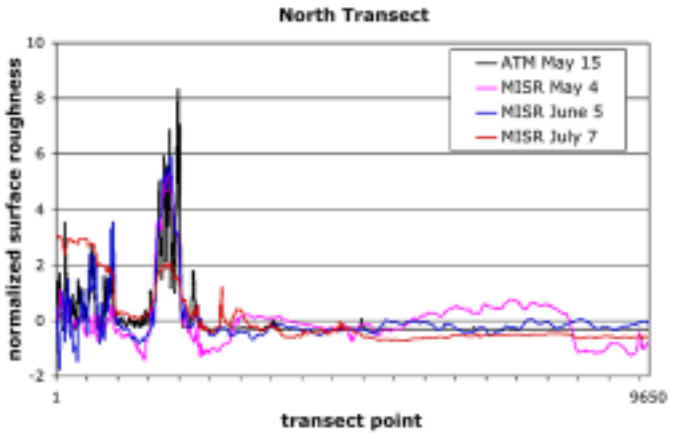

Fig. 9. Comparison of ATM and MISR normalized surface roughness for the north transect.

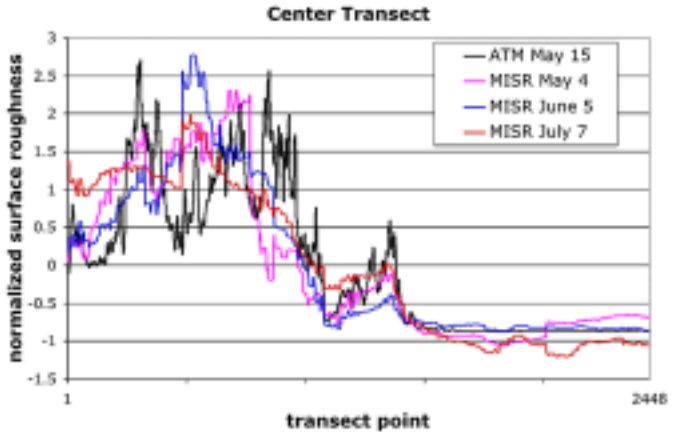

Fig. 10. Comparison of ATM and MISR normalized surface roughness for the center transect.

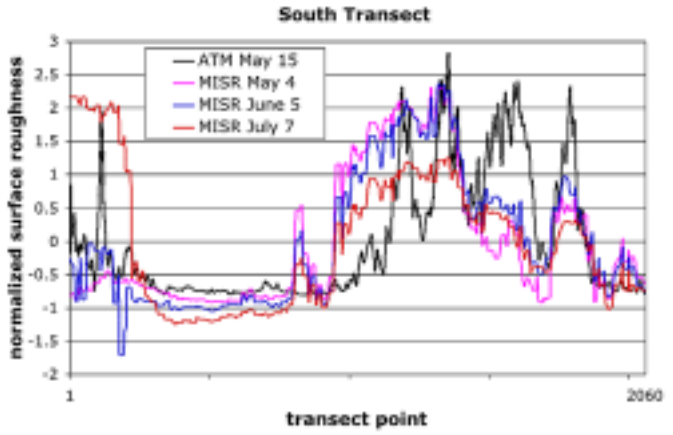

Fig. 11. Comparison of ATM and MISR normalized surface roughness for the south transect.

melt ponds have formed over an extensive area of the basin, and the glacier terminus becomes active, injecting icebergs into the narrow bay. The highest areas of the drainage basin (above nearly 2000 m) remain mostly smooth, likely due to the lack of surface melt.

Figs. 9–11 show the normalized surface roughness values for the north, central, and south transects, respectively. In these figures, MISR NDAI values from all three images are shown.

TABLE III
CORRELATIONS (R^2) BETWEEN ATM AND MISR NORMALIZED SURFACE ROUGHNESS VALUES

Transect Location	4 May 2001	5 June 2001	7 July 2001
North	0.46	0.62	0.36
Central	0.69	0.69	0.74
South	0.27	0.46	0.27

Correlations between MISR NDAI and ATM surface roughness values are given in Table III. MISR normalized surface roughness values for May and June most closely resemble the ATM values. This is expected, since they are from about the same time in the summer as the ATM data acquisitions. Differences in the first part of the transect may possibly be attributed to ice surges or changes in glacier mass balance that would affect roughness. Such changes have been documented by [35] and show that, over the period of 1993–1998, the Jakobshavn Glacier appeared to be thickening, in sharp contrast to most other outlet glaciers of Greenland. By July, reflectances over the lower reaches of the glacier have decreased, and melt ponds are visible in the image, indicating that substantial melting is underway. Additional measurements from automated weather stations in the Jakobshavn ablation region indicate above-freezing temperatures and snow/firn ablation starting in late June. In the central transect, the lower portion of the glacier becomes significantly rougher in July. In this region, it is likely that the snow bridges previously spanning the crevasses would have melted out, revealing a rougher surface at a spatial scale that is detectable by MISR.

The roughness measurements are in general agreement with measurements made by [37] in which they show distinct differences in surface roughness between surveyed areas in the lower central ice stream (corresponding to the lower part of the center ATM transect, dominated by irregularly oriented crevasses and seracs), an area to the north of the ice stream (corresponding to the lower portion of the north ATM transect, dominated by lineated crevasses), and a third area located to the south of the central ice stream (corresponding to the lower portion of the south transect, dominated by sastrugi and melt-related features such as melt ponds).

C. Blue-Ice Areas in Antarctica

The various normalized difference images each emphasize a different aspect of the MISR image of the region. We have created a three-band false-color image by combining the NDAI image (in which the contrast was reversed to make smooth areas brighter than rough areas) with the Blue-Red normalized difference image and the IR-blue normalized difference image. The BRND image emphasizes the blue-ice areas because of their peak reflectance in the blue wavelengths. The IBND image further emphasizes the difference between blue ice and snow based on grain size. It is the angular information, however, that provides a means of distinguishing between crevassed blue ice and smooth blue ice. This can be seen in Fig. 12 where Red = NDAI, Green = BRND, and Blue = IBND. Here, the blue-ice areas are displayed as pink, easily separated from the crevassed glacier regions that appear yellow-orange. The Darwin Glacier is shown to have surface characteristics similar to the other smooth blue-ice areas. We speculate that this is because it has very slow velocity and high ablation rates when compared with the other glaciers in the region. This would cause the surface to remain relatively smooth at the MISR scale.

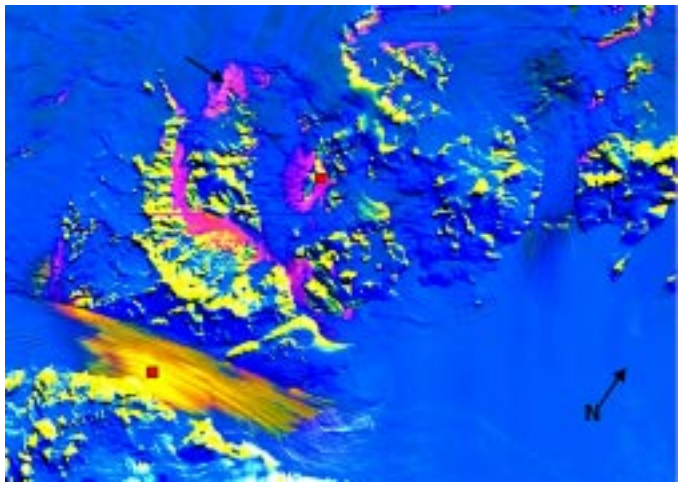

Fig. 12. False-color image of blue-ice areas and glaciers from MISR. Red is the back-fore normalized difference. Green is the blue-red normalized difference. Blue is the near-infrared-blue normalized difference. Blue ice areas are pink. The red squares show the pixels that were used to create the normalized BRF plots. The "Meteorite Hills" area (photo in Fig. 4) is indicated by the black arrow.

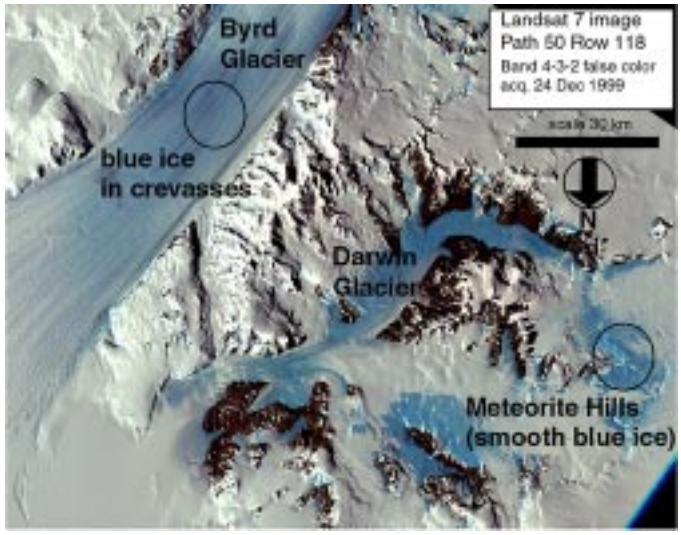

Fig. 13. Landsat TM true-color image of blue-ice areas. Rock outcrops show dark. Both smooth and crevassed blue ice are shown as darker blue, while snow and firn are white.

For comparison with the MISR image, we also show a Landsat TM image at 30-m spatial resolution that covers roughly the same area as the MISR image (Fig. 13). In this image, the blue-ice areas appear darker blue, while the snow appears gray-white. Even with enhanced spatial resolution, there is no spectrally based ability to distinguish between crevassed blue ice (such as Byrd Glacier) and the smooth blue ice (such as Meteorite Hills).

To provide some perspective on the "smoothness" of the smooth blue ice, recent work [52] describes the surface roughness of blue ice in a region of Dronning Maud Land, Antarctica. Measurements in [52] indicate a ripple height (trough-to-crest)

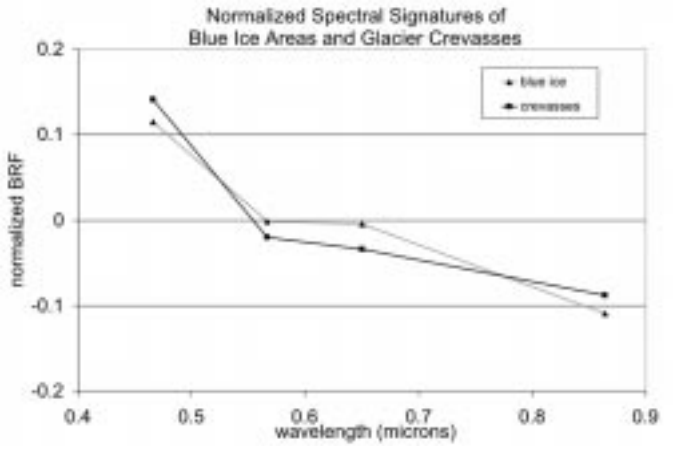

Fig. 14. Normalized spectral signatures of glacier crevasses and blue-ice areas. Only very small differences are evident indicating that, at the MISR wavelengths, these surface types are not easily distinguished.

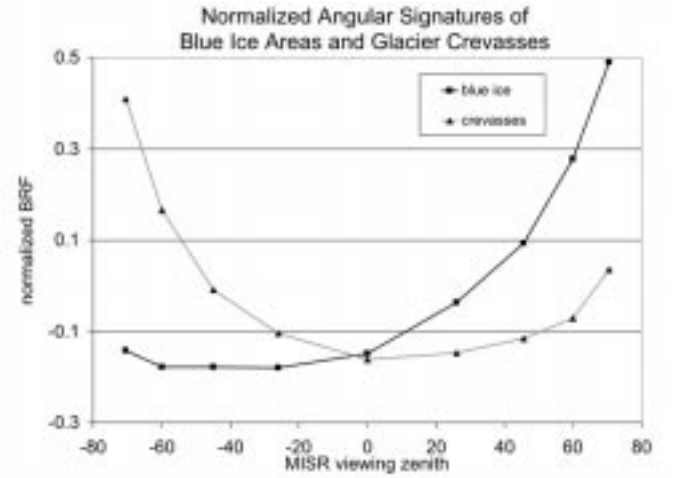

Fig. 15. Normalized angular signatures of blue ice and glacier crevasses. Blue ice is forward scattering, while crevasses are backward scattering. The surfaces are clearly distinguishable at the MISR viewing zeniths.

of about 2 cm and a wavelength of about 20–25 cm. Such texture does not appear to be detectable at the scale of the MISR pixel.

Normalized BRFs for smooth and crevassed blue ice demonstrate more fully the differences between their angular and spectral signatures. We first extracted a set of 50 pixels from each area and computed the mean BRF for each. We then normalized them according to (2) and plotted the spectral and angular curves. Fig. 14 shows the normalized BRFs in the four nadir MISR channels for both blue ice and glacier crevasses. Spectrally, there is very little difference between the two at the MISR wavelengths. This is in sharp contrast to the very different angular signatures shown in Fig. 15. It is not the goal of this preliminary work to do so, but with such a clear distinction, a relatively simple, yet highly accurate, algorithm may be derived for mapping ablation-derived blue-ice extent over the entire continent. While the MISR spectral channels are not optimized for detecting spectral differences it is unlikely that any spectrally based method would be able to easily distinguish between smooth blue ice and crevassed blue ice, since they have the same material properties, but with a different configuration and surface roughness.

VI. Conclusions

We have demonstrated that MISR data may be used to characterize surface roughness on sea ice and ice sheets. In the sea ice example, an unsupervised classification of the MISR angular data indicates that these data can be used to distinguish between multiyear and first-year ice types. While it is not as clear a delineation as with SAR data, this is a demonstration that multiangular optical data can provide additional information. In cases where surface melt is occurring and SAR data are less useful, multiangular optical data could provide key ice-mapping information.

Over the Jakobshavn Glacier, statistically significant correlations were found between surface roughness values derived from airborne laser altimeter measurements and a proxy estimate of surface roughness from MISR. With additional research and validation efforts, characterization of areas on the basis of their surface roughness would be able to provide characterization of regions of smooth dry snow, sastrugi, regions of melt ponds and ablation channels, and heavily crevassed ice regions. Comparison of surface roughness patterns over the course of the summer season leads to a better understanding of ice-surface morphogenetic processes, such as the interaction of wind and ablation processes that are important for understanding ice sheet mass balance.

In the Antarctic case study, we found multiangular data to be uniquely able to characterize ice surfaces on the basis of their surface roughness. Smooth blue-ice areas, so difficult to detect with multispectral methods, are clearly distinguished from crevassed blue ice when multiangular data are used. Future applications might include continentwide mapping of blue-ice areas to examine intraannual and interannual variability within the context of climate change studies.

These preliminary results indicate that additional studies are warranted. A number of outstanding questions remain, including understanding the spatial scale at which roughness is detected by MISR and how solar illumination and feature orientation play into this. Comprehensive studies are needed that relate snow and ice angular signatures, surface texture, and key geophysical parameters. MISR also appears to be highly effective at discriminating clouds from snow and ice (including thin clouds such as cirrus, which are particularly difficult to detect) based on a combination of angular and spectral properties [53]. Future research is needed to quantify the level of accuracy of cloud detection over snow and ice.

As a proof-of-concept, the MISR instrument has demonstrated its success in multiangular mapping of sea ice and ice sheet surfaces. However, with only a 380-km swath width, applications are limited to regional scales or multitemporal composites. High temporal resolution multiangular data are needed to provide daily observations of the climatically sensitive polar regions. Synergies between MISR and instruments with more frequent coverage, such as the Moderate Resolution Imaging Spectroradiometer (MODIS), will need to be exploited to optimize the blend of spatial coverage with innovative multiangular approaches.

Acknowledgment

MISR data were provided through the NASA Langley Distributed Active Archive Center. Sea ice charts were pro-

vided through the National Ice Center, Washington, D.C. The authors thank Dr. W. Krabill, NASA Wallops Flight Facility for providing the ATM laser altimetry data. The authors are also grateful to Dr. J. Box, University of Colorado and NASA's Program for Arctic Regional Climate Assessment (PARCA) for providing temperature and surface height data for sites within the Jakobshavn Glacier ablation region. The authors thank U. Herzfeld for useful discussions on characterizing ice sheet surface roughness and the reviewers, whose comments made substantial improvements to this paper.

REFERENCES

[1] D. J. Diner, G. P. Asner, R. Davies, Y. Knyazikhin, J-P. Muller, A. W. Nolin, B. Pinty, C. B. Schaaf, and J. Stroeve, "New directions in Earth observing: Scientific applications of multiangle remote sensing," *Bull. Amer. Meteorol. Soc.*, vol. 80, pp. 2209–2228, 1999.

[2] A. Nolin and S. Liang, "Progress in bidirectional reflectance modeling and applications for surface particulate media: Snow and soils," *Remote Sens. Rev.*, vol. 18, pp. 307–342, 2000.

[3] S. A. W. Gerstl, W. Gebauer, C. C. Borel, and C. Dochitoiu, "Angular signature retrieval and comparison with spectral signatures from AirMISR data," in *Proc. IGARSS*, vol. AA10-09, 1999, pp. 74–76.

[4] U. C. Herzfeld, H. Mayer, W. Feller, and M. Mimler, "Glacier roughness surveys of Jakobshavn Isbrae drainage basin, West Greenland, and morphological characterization," *Zeitschrift Gletscherkunde Glazioalgeol.*, vol. 35, pp. 117–146, 1999.

[5] S. G. Warren, R. E. Brandt, and P. O'Rawe Hinton, "Effect of surface roughness on bi-directional reflectance of Antarctic snow," *J. Geophys. Res.*, vol. 103, pp. 25789–25807, 1998.

[6] W. T. Pfeffer and C. S. Bretherton, "The effect of crevasses on the solar heating of a glacier surface," in *Proc. IAHS Vancouver Symp.: Physical Basis Ice Sheet Model.*, 1987, pp. 191–205.

[7] R. Kwok, E. Rignot, B. Holt, and R. Onstott, "Identification of sea ice types in spaceborne synthetic aperture radar data," *J. Geophys. Res.*, vol. 97, pp. 2391–2402, 1992.

[8] C. Tsatsoulis and R. Kwok, *Analysis of SAR Data of the Polar Oceans: Recent Advances*. Berlin, Germany: Springer-Verlag, 1998.

[9] R. M. Goldstein, H. Engelhardt, B. Kamb, and R. M. Frolich, "Satellite radar interferometry for monitoring ice-sheet motion: Application to an Antarctic ice stream," *Science*, vol. 262, p. 1525, 1993.

[10] I. Joughin, D. P. Winebrenner, and M. A. Fahnestock, "Observations of complex ice sheet motion in Greenland using satellite radar interferometry," *Geophys. Res. Lett.*, vol. 22, pp. 571–574, 1995.

[11] I. Joughin, D. Winebrenner, M. Fahnestock, R. Kwok, and W. Krabill, "Measurement of ice-sheet topography using satellite radar interferometry," *J. Glaciol.*, vol. 42, pp. 10–22, 1996.

[12] E. Rignot, S. Gogineni, W. Krabill, and S. Ekholm, "Ice discharge from north and northeast Greenland as observed from satellite radar interferometry," *Science*, vol. 276, pp. 934–937, 1997.

[13] D. J. Diner, C. J. Bruegge, J. V. Martonchik, G. W. Bothwell, E. D. Danielson, E. L. Floyd, V. G. Ford, L. E. Hovland, K. L. Jones, and M. L. White, "A multiangle imaging spectroradiometer for terrestrial remote sensing from the earth observing system," *Int. J. Imaging Syst. Technol.*, vol. 3, pp. 92–107, 1991.

[14] P. Gloersen and W. J. Campbell, "Recent variations in Arctic and Antarctic sea-ice covers," *Nature*, vol. 352, pp. 4–13, 1991.

[15] W. L. Chapman and J. E. Walsh, "Recent variations of sea ice and air temperature in high latitudes," *Bull. Amer. Meteorol. Soc.*, vol. 74, pp. 33–47, 1993.

[16] E. Bjorgo, O. M. Johannessen, and M. W. Miles, "Analysis of merged SSMR-SSMI time series of Arctic and Antarctic sea ice parameters 1978–1995," *Geophys. Res. Lett.*, vol. 24, pp. 413–416, 1997.

[17] J. A. Maslanik, M. C. Serreze, and R. G. Barry, "Recent decreases in Arctic summer ice cover and linkages to atmospheric circulation anomalies," *Geophys. Res. Lett.*, vol. 23, pp. 1677–1680, 1996.

[18] D. J. Cavalieri, P. Gloersen, C. L. Parkinson, and J. C. Comiso, "Observed hemispheric asymmetry in global sea ice changes," *Science*, vol. 278, pp. 1104–1106, 1997.

[19] W. B. I. Tucker, J. W. Weatherly, D. T. Eppler, L. D. Farmer, and D. L. Bentley, "Evidence for rapid thinning of sea ice in the western Arctic Ocean at the end of the 1980s," *Geophys. Res. Lett.*, vol. 28, pp. 2851–2854, 2001.

[20] D. A. Rothrock, Y. Yu, and G. A. Maykut, "Thinning of the Arctic sea-ice cover," *Geophys. Res. Lett.*, vol. 26, pp. 3469–3472, 1999.

[21] J. C. Comiso and R. Kwok, "Surface and radiative characteristics of the summer arctic sea ice cover from multi-sensor satellite observations," *J. Geophys. Res.*, vol. 101, pp. 28 397–28416, 1996.

[22] C. Bertoia, J. Falkingham, and F. Fetterer, "Polar SAR data for operational sea ice mapping," in *Analysis of SAR Data of the Polar Oceans*, C. Tsatsoulis and R. Kwok, Eds. Berlin, Germany: Springer-Verlag, 1998, pp. 201–234.

[23] R. Kwok, "The RADARSAT geophysical processor system," in *Analysis of SAR Data of the Polar Oceans*, C. Tsatsoulis and R. Kwok, Eds. Berlin, Germany: Springer-Verlag, 1998, pp. 235–258.

[24] K. R. Dedrick, K. Partington, M. V. Woert, C. A. Bertoia, and D. Benner, "U.S. National/Naval Ice Center digital sea ice data and climatology," *Can. J. Remote Sens.*, vol. 27, pp. 457–475, 2001.

[25] R. G. Onstott, "SAR and scatterometer signatures of sea ice," in *Microwave Remote Sensing of Sea Ice*, F. D. Carsey, Ed. Washington, D.C.: American Geophysical Union, 1992, pp. 73–104.

[26] R. Kwok, E. Rignot, B. Holt, and R. Onstott, "Identification of sea ice types in spaceborne synthetic aperture radar data," *J. Geophys. Res.*, vol. 97, pp. 2391–2402, 1992.

[27] F. M. Fetterer, D. Gineris, and R. Kwok, "Sea ice type maps from Alaska Synthetic Aperture Radar Facility imagery: An assessment," *J. Geophys. Res.*, vol. 99, pp. 22 443–22 458, 1994.

[28] S. G. Beaven, S. P. Gogineni, and M. Shanableh, "Radar backscatter signature of thin ice in the central Arctic," *Int. J. Remote Sens.*, vol. 15, pp. 1149–1154, 1994.

[29] R. J. Gurney, J. L. Foster, and C. L. Parkinson, *Atlas of Satellite Observations Related to Global Change*. Cambridge, U.K.: Cambridge Univ. Press, 1993, p. 470.

[30] A. Ohmura and N. Reeh, "New precipitation and accumulation maps for Greenland," *J. Glaciol.*, vol. 37, pp. 140–148, 1991.

[31] J. R. McConnell, E. Mosley-Thompson, D. H. Bromwich, R. C. Bales, and J. D. Kyne, "Interannual variations of snow accumulation on the Greenland ice sheet (1985–1996): New observations versus model predictions," *J. Geophys. Res.*, vol. 105, pp. 4039–4046, 2000.

[32] E. Mosley-Thompson, J. R. McConnell, R. C. Bales, Z. Li, P.-N. Lin, K. Steffen, L. G. Thompson, R. Edwards, and D. Bathke, "Local to regional-scale variability of Greenland accumulation from PARCA cores," *J. Geophys. Res.*, vol. 106, pp. 33839–33851, 2001.

[33] R. C. Bales, J. R. McConnell, and E. Mosley-Thompson, "Accumulation map of the Greenland ice sheet: 1971–1990," *Geophys. Res. Lett.*, vol. 28, pp. 2967–2970, 2001.

[34] W. Abdalati and K. Steffen, "Snowmelt on the Greenland ice sheet as derived from passive microwave satellite data," *J. Climate*, vol. 10, pp. 165–175, 1997.

[35] W. Krabill, E. Frederick, S. Manizade, C. Martin, J. Sonntag, R. Swift, R. Thomas, W. Wright, and J. Yungel, "Rapid thinning of parts of the southern Greenland ice sheet," *Science*, vol. 283, pp. 1522–1524, 1999.

[36] W. Krabill, R. Thomas, K. Jezek, K. Kuivinen, and S. Manizade, "Greenland ice sheet thickness changes measured by laser altimetry," *Geophys. Res. Lett.*, vol. 22, pp. 2341–2344, 1995.

[37] U. C. Herzfeld, M. Stauber, and N. Stahl, "Geostatistical characterization of ice surfaces from ERS-1 and ERS-2 SAR data, Jakobshavn Isbrae, Greenland," *Ann. Glaciol.*, vol. 30, pp. 224–234, 2000.

[38] V. Schytt, "Glaciology II. Blue ice-fields, moraine features, and glacier fluctuations," *Norwegian–British–Swedish Antarctic Expedition, 1949–1952 Scientific Results*, vol. 4E, pp. 183–204, 1961.

[39] R. Bintanja, S. Jonsson, and W. H. Knap, "The annual cycle of the surface energy balance of Antarctic blue ice," *J. Geophys. Res.*, vol. 102, pp. 1867–1881, 1997.

[40] R. Bintanja, "On the glaciological, meteorological, and climatological significance of Antarctic blue ice areas," *Rev. Geophys.*, vol. 37, pp. 337–359, 1999.

[41] R. Bintanja and C. H. Reijmer, "Meteorological conditions over Antarctic blue-ice areas and their influence on the local surface mass balance," *J. Glaciol.*, vol. 47, pp. 37–50, 2001.

[42] M. Yoshida, H. Ando, K. Omoto, and Y. Ageta, "Discovery of meteorites near Yamoto Mountains, East Antarctica," *Antarctic Rec.*, vol. 39, pp. 62–65, 1971.

[43] W. A. Cassidy, R. Harvey, J. Schutt, G. DeLisle, and K. Yanai, "The meteorite collection sites of Antarctica," *Meteoritics*, vol. 27, pp. 490–525, 1992.

[44] M. Mellor and C. Swithinbank, "Airfields on Antarctic glacier ice," CRREL, Hanover, NH, Rep. 89-21, 1989.

[45] O. Orheim and B. Lucchitta, "Investigating climate change by digital analysis of blue ice extent on satellite images of Antarctica," *Ann. Glaciol.*, vol. 14, pp. 211–215, 1990.

[46] R. Bintanja and M. R. van den Broeke, "The climate sensitivity of Antarctic blue-ice areas," *Ann. Glaciol.*, vol. 21, pp. 157–161, 1995.
[47] J.-G. Winther, M. N. Jespersen, and G. E. Liston, "Blue-ice areas in Antarctica derived from NOAA AVHRR satellite data," *J. Glaciol.*, vol. 47, pp. 325–334, 2001.
[48] R. O. Duda and P. E. Hart, *Pattern Classification and Scene Analysis*. New York: Wiley, 1973, p. 482.
[49] S. G. Warren, "Optical properties of snow," *Rev. Geophys. Space Phys.*, vol. 20, pp. 67–89, 1982.
[50] J. Dozier and D. Marks, "Snow mapping and classification from Landsat Thematic Mapper data," *Ann. Glaciol.*, vol. 9, pp. 97–103, 1987.
[51] A. W. Nolin and J. Dozier, "A hyperspectral method for remotely sensing the grain size of snow," *Remote Sens. Environ.*, vol. 74, pp. 207–216, 2000.
[52] R. Bintanja, C. H. Reijmer, and S. J. M. H. Hulscher, "Detailed observations of the rippled surface of Antarctic blue-ice areas," *J. Glaciol.*, vol. 47, pp. 387–396, 2001.
[53] G. Zhao and L. DiGirolamo, "Cloud detection with the mulitangle imaging spectroradiometer (MISR)," *EOS Trans.*, vol. AGU 81, no. 48, Fall 2000.

Anne W. Nolin received the B.A. degree in anthropology and the M.S. degree in soils, water, and engineering from the University of Arizona, Tucson, in 1980 and 1987, respectively. She received the Ph.D. degree in geography from the University of California, Santa Barbara, in 1993.

She is currently Member of the MISR Science Team at the Jet Propulsion Laboratory, Pasadena, CA. She has worked as a Research Scientist at the Cooperative Institute for Research in Environmental Sciences and the National Snow and Ice Data Center at the University of Colorado, Boulder, since 1993. Her research interests include integrating studies of snow, hydrology, and climate with innovative methods of satellite observation.

Dr. Nolin is a member of the Association of American Geographers, the American Meteorological Society, the International Glaciological Society, and the American Geophysical Union. As part of the MISR Science Team, she received a NASA Group Achievement Award.

Florence M. Fetterer (M'89) received the B.A. degree from St. John's College, Annapolis, MD, in 1981 and the M.S. degree in physical oceanography from Old Dominion University, Norfolk, VA, in 1985.

She has worked as the NOAA Liaison for the National Snow and Ice Data Center at the University of Colorado, Boulder, since 1996. Previously, she was a Remote Sensing Scientist for the Naval Research Laboratory, Stennis Space Center, Hattiesburg, MI. Her research interests include applications-oriented remote sensing of sea ice.

Ms. Fetterer has been affiliate member of the remote sensing section of the IEEE since 1989 and is a member of the American Geophysical Union.

Theodore A. Scambos received the B.S. degree in geology from the State University of Stony Brook, Stony Brook, NY, in 1977, the M.S. degree in geology from Virginia Polytechnic Institute and State University, Blacksburg, in 1980, and the Ph.D. degree in geology from the University of Colorado, Boulder, in 1991.

Currently, he is investigating ice shelf stability and the history of ice flow in the Antarctic, as well as developing new ways to use satellite data to gather information about ice sheets. He has worked at the National Snow and Ice Data Center at the University of Colorado since 1993 and was previously a contractor at NASA's Goddard Space Flight Center for three years.

Dr. Scambos is a member of the International Glaciological Society and the American Geophysical Union.